CHEMICAL PHYSICS

Under-expanded supersonic CO_2 freezing jets during champagne cork popping

Gérard Liger-Belair[1]*, Daniel Cordier[1], Robert Georges[2]

During champagne cork popping, the CO_2/H_2O gas mixture initially under pressure in the bottleneck freely expands into ambient air and experiences adiabatic cooling. A comparison between the condensation phenomena accompanying cork popping from bottles stored at 20° and 30°C was made. The initial headspace-to-ambient-pressure ratio much exceeded the critical ratio needed for the gas mixture to reach Mach 1, thus forming under-expanded supersonic CO_2 freezing jets expelled from the throat of the bottlenecks. It was emphasized that, after adiabatic cooling and with a saturation ratio for gas-phase CO_2 about twice higher for the bottles stored at 30°C, dry ice CO_2 clusters grow bigger and reach the critical size needed to achieve the Mie scattering of light. Moreover, during the very first millisecond following cork popping, evanescent normal shock waves (or Mach disks) were unveiled in the jets, until the reservoir-to-ambient-pressure ratio goes below a critical ratio.

INTRODUCTION

Even if it is far safer and advised to uncork a champagne bottle with a subdued sigh to prevent serious eye injuries (*1*–*4*), uncorking a bottle with a bang has become a festive and iconic action preceding champagne tasting. Champagne and sparkling wines elaborated through the same traditional method are indeed under a high pressure of carbon dioxide (CO_2), as gas-phase CO_2 forms together with ethanol during a second in-bottle fermentation process promoted by adding yeasts and a certain amount of sugar in bottles hermetically sealed with a crown cap or a cork stopper (*5*, *6*). This is a basic application of Henry's law, which states that the concentration of dissolved CO_2 in the liquid phase is proportional to the partial pressure of gas-phase CO_2 in the bottleneck. Therefore, during the cork popping process, a plume mainly composed of gas-phase CO_2 (with traces of water vapor) freely expands out of the bottleneck through ambient air. The commonly accepted idea behind champagne cork popping was that the gas mixture gushing from the bottleneck experiences adiabatic expansion and therefore cools adjacent air packages beyond the water dew point. Condensation or even freezing of water vapor found in ambient air can therefore be observed in the form of a characteristic gray-white cloud of fog (*7*–*9*). The gray-white color is characteristic of Mie scattering (i.e., the scattering of light by particles with typical sizes larger than the wavelength), well known to be at the origin of cloud color in the sky (*10*).

Recently, cork popping from clear transparent bottles of champagne stored at different temperatures (namely, 6°, 12°, and 20°C) was filmed through high-speed video imaging (*11*). On the basis of this set of experiments, the situation has appeared really more complex and subtle than described before. The key role of the champagne temperature was pointed out. It was found that, somewhat counterintuitively, the higher the initial temperature of champagne before cork popping, the lower the temperature reached by the gas mixture freely expanding above the bottleneck after adiabatic cooling. For the bottles stored at 20°C (under a pressure close to 7.5 bar), the temperature of the CO_2/H_2O gas mixture fell close to −90°C after adiabatic cooling and therefore below the freezing temperature of gas-phase CO_2 under 1 bar. Under these conditions, the characteristic gray-white cloud of fog classically observed above the bottlenecks of bottles stored at lower temperatures completely disappeared and was replaced by a more evanescent and unexpectedly blue plume. Blue haze is indeed typical of Rayleigh scattering, which describes the elastic scattering of light by particles much smaller than the wavelength of light (*10*). Depending on the strongly bottle temperature–dependent saturation ratio experienced by gas-phase CO_2 after adiabatic expansion, it was emphasized that blue haze is the signature of a partial and transient heterogeneous freezing of gas phase CO_2 on ice water clusters homogeneously nucleated in the bottlenecks (*11*).

Here, the role of temperature was still more deeply investigated as the CO_2/H_2O gas mixture initially under pressure in the bottlenecks freely expands during champagne cork popping. A comparison between the condensation phenomena accompanying cork popping from bottles stored at 20° and 30°C was made. Unlike the deep blue haze observed for the cork popping bottles stored at 20°C, heterogeneous freezing of gas-phase CO_2 turned white for the 30°C bottles. Moreover, closer examination of the freezing plumes expanding from the champagne bottlenecks revealed another notable feature well known in aircraft and aerospace engineering. From a phenomenological perspective, a parallel between the CO_2/H_2O gas mixture freely expanding from a champagne bottleneck while cork popping and the phenomena arising in a rocket plume exhaust was done.

RESULTS AND DISCUSSION

Temperature dependence of heterogeneous CO_2 freezing plumes

Time sequences displayed in Fig. 1 illustrate minute details of the cork popping process as seen through high-speed video imaging for bottles stored at 20° and 30°C, respectively. As already unveiled in a previous study, for the bottle stored at 20°C, a blue plume appears about 250 μs after the cork popping process and develops above the bottleneck for several milliseconds until it progressively vanishes. It was emphasized that blue haze is the signature of a partial and transient heterogeneous freezing of gas-phase CO_2 on ice water clusters homogeneously nucleated in the bottlenecks (*11*). Blue haze is indeed typical of the Rayleigh scattering of light by clusters much smaller than the wavelengths of ambient light ranging from 0.4 to 0.8 μm. For the bottle stored at 30°C, the CO_2 freezing plume gushing from the bottleneck appears much more rapidly, in the very first microseconds following the cork popping

[1]Equipe Effervescence, Champagne et Applications (GSMA - UMR CNRS 7331), Université de Reims Champagne-Ardenne, UFR Sciences Exactes et Naturelles, BP 1039, 51687 Reims Cedex 2, France. [2]Institut de Physique de Rennes, UMR CNRS 6251, Université de Rennes 1, Campus de Beaulieu, 35042 Rennes, France.
*Corresponding author. Email: gerard.liger-belair@univ-reims.fr

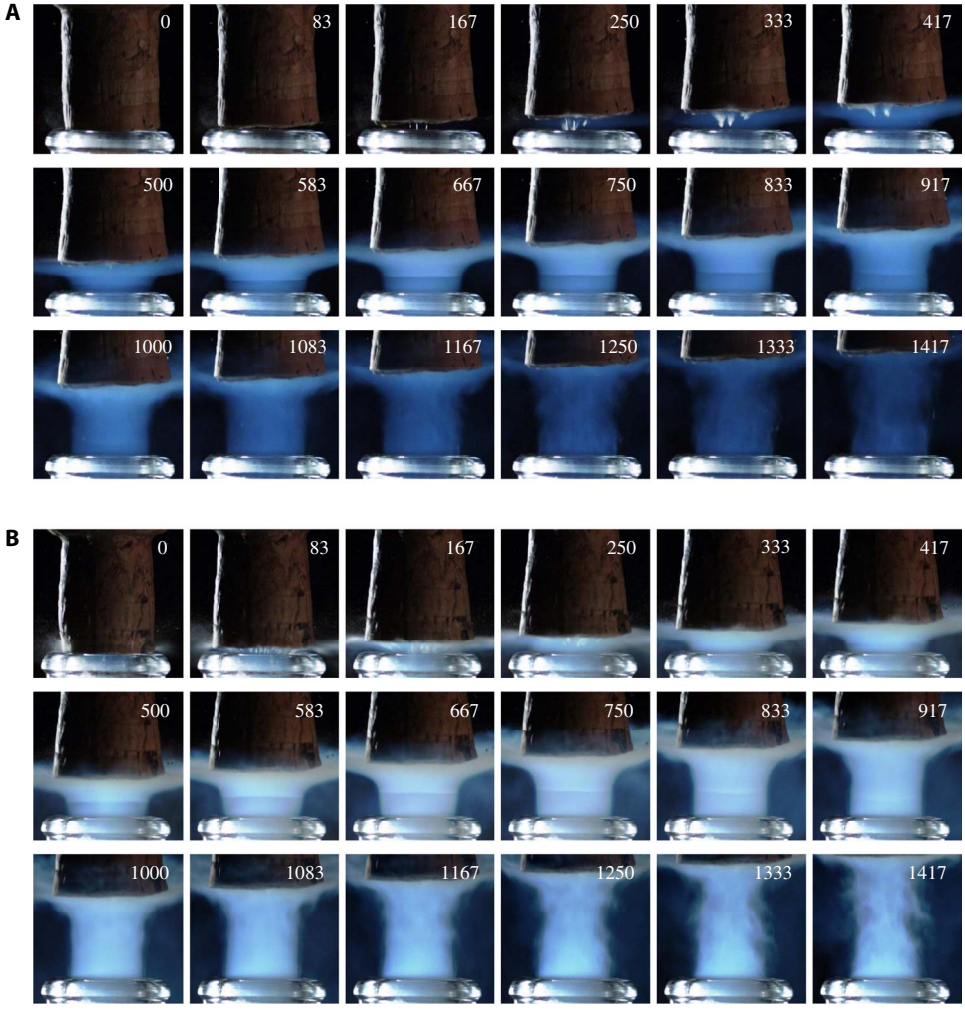

Fig. 1. High-speed video imaging of CO_2 freezing jets formed during champagne cork popping. Time sequences showing the freezing jet expelled from the throat of a bottleneck for a bottle stored at 20°C (**A**) as compared with that expelled from a bottle stored at 30°C (**B**). The time elapsed after cork popping appears in each panel (in microseconds).

process, and seems to be optically more opaque than the blue haze freely expanding from the bottle stored at 20°C. Moreover, the color of the plume expelled from the bottle stored at 30°C rather turns gray-white, a tint which is a characteristic of Mie scattering (as the size of the scattering clusters becomes comparable or larger in size than the wavelengths of ambient light). Why such a modification of the global aspect of the CO_2 freezing plume expelled from the throat of the bottleneck as the bottle's temperature increases?

Adiabatic expansion and its drop of temperature is the mechanism behind the formation of the CO_2 freezing plume observed during the cork popping process. The drop of temperature experienced by the CO_2/H_2O gas mixture, initially under pressure in the bottleneck and freely expanding above the bottleneck, classically obeys the following equation

$$T_f = T \times \left(\frac{P_0}{P_{CB}}\right)^{\frac{\gamma-1}{\gamma}} \quad (1)$$

with T and P_{CB} being the initial temperature and pressure of the CO_2/H_2O gas mixture, respectively, before cork popping (in the sealed bottle); T_f and P_0 being the final temperature and pressure, respectively, reached by the CO_2/H_2O gas mixture after adiabatic expansion; and γ being the ratio of specific heats of the gas mixture experiencing adiabatic expansion (mostly made of gas-phase CO_2 and therefore being equal to 1.3) (*12*).

In Fig. 2, the respective partial pressures of both gas-phase CO_2 and water vapor in a champagne corked bottle are plotted as a function of the bottle's temperature T, as determined in accordance with the thermodynamic equilibrium (see Materials and Methods). The temperature-dependent partial pressure of gas-phase CO_2 being more than two orders of magnitude higher than that of water vapor pressure, the total pressure P_{CB} of the CO_2/H_2O gas mixture found in the sealed bottles is therefore considered as being equivalent to the partial pressure of gas-phase CO_2. In the range of temperatures between 20° and 30°C, the pressure of the gas mixture in the headspace of the sealed bottles ranges between approximately 7.5 and 10.2 bar, as shown in Fig. 2. After adiabatic expansion, the pressure within the bottleneck falls to atmospheric pressure, close to 1 bar. CO_2 being the major component of the CO_2/H_2O freely expanding gas mixture, its partial pressure therefore falls close to 1 bar, whatever the bottle temperature. With regard to

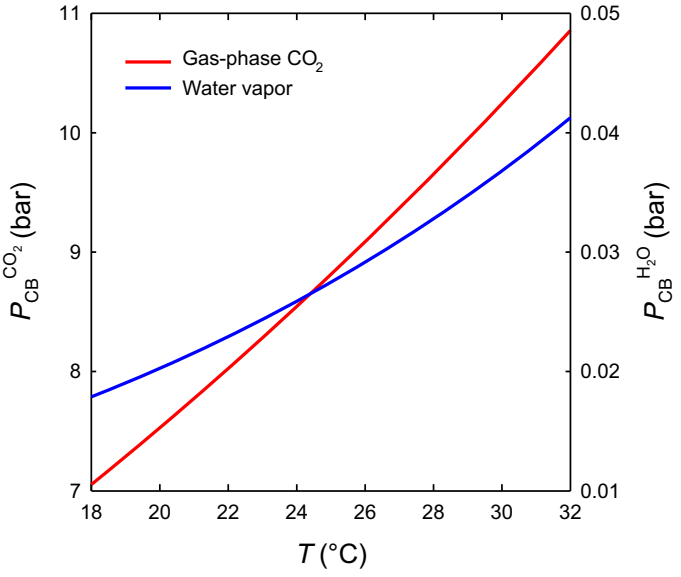

Fig. 2. Partial pressures (in bar) of both gas-phase CO_2 and water vapor found in the headspace of a corked bottle in equilibrium with the liquid phase, as a function of the bottle's temperature (in °C).

the partial pressure of water vapor after adiabatic expansion, it drops to respectively about 2.7×10^{-3} and 3.6×10^{-3} bar, whether the bottle temperature is 20° or 30°C (see Table 1). By combining Eqs. 1 and 11, the final temperature T_f reached by the CO_2/H_2O gas mixture after adiabatic expansion can therefore be determined as a function of all the parameters of the sealed bottle (i.e., before cork popping) according to the following relationship

$$T_f = T^{\frac{2-\gamma}{\gamma}} \left(\frac{P_0 (V_G + k_H R T V_L)^2}{n_T k_H R^2 V_L} \right)^{\frac{\gamma-1}{\gamma}} \quad (2)$$

Moreover, the huge drop of temperature experienced by the CO_2/H_2O gas mixture after adiabatic expansion has some strong effects on the respective saturated vapor pressures of both CO_2 and water. At the temperatures reached by the CO_2/H_2O gas mixture after adiabatic expansion (−89° and −95°C, respectively, whether the bottle's temperature is 20° or 30°C), and with the knowledge of the respective partial pressures of both water vapor and gas-phase CO_2 combined with their corresponding saturated vapor pressures, as determined through Eqs. 13 and 14, respectively, the saturation ratios of both gas-phase CO_2 and water vapor (i.e., $S_{CO_2} = P_{vap}^{CO_2}/P_{sat}^{CO_2}$ and $S_{H_2O} = P_{vap}^{H_2O}/P_{sat}^{H_2O}$, respectively) can be determined (see Table 1). After the CO_2/H_2O gas mixture has achieved adiabatic expansion, the saturation ratios reached by water vapor are huge (about 23,800 and 113,800, whether the bottle was stored at 20° or 30°C). Comparatively, the saturation ratios reached by gas-phase CO_2 are indeed much smaller but still higher than unity (about 2.5 for the bottles stored at 20°C and about 4.8 for the bottles stored at 30°C). With saturation ratios higher than unity after adiabatic expansion, phase change becomes thermodynamically favorable. Water vapor could therefore transform into ice water clusters, whereas gas-phase CO_2 could transform into dry ice CO_2 clusters (for the bottles stored at 20° and 30°C).

To further understand the differences observed between the freezing plumes freely expanding from the cork popping bottles

Table 1. Parameters of the CO_2/H_2O gas mixture found in the bottlenecks of the bottles stored at 20° and 30°C before cork popping and after adiabatic expansion.

Storage temperature of bottles (in K)	293	303
Pressure of gas-phase CO_2 in the sealed bottle, $P_{CB}^{CO_2}$ (in bar)	7.5	10.2
Pressure of water vapor in the sealed bottle, $P_{CB}^{H_2O}$ (in bar)	0.0203	0.0368
Temperature reached by the gas mixture in the bottleneck after adiabatic expansion, T_f (in K)	183.9	177.1
Pressure of gas-phase CO_2 in the bottleneck after adiabatic expansion, $P_{vap}^{CO_2}$ (in bar)	1	1
Pressure of water vapor in the bottleneck after adiabatic expansion, $P_{vap}^{H_2O}$ (in bar)	0.0027	0.0036
Saturated vapor pressure of gas-phase CO_2 after adiabatic expansion, $P_{sat}^{CO_2}$ (in bar)	0.39	0.21
Saturated vapor pressure of ice water after adiabatic expansion, $P_{sat}^{H_2O}$ (in Pa)	0.011	0.003
Saturation ratio of gas-phase CO_2 after adiabatic expansion, S_{CO_2}	2.53	4.84
Saturation ratio of water vapor after adiabatic expansion, S_{H_2O}	≈23,800	≈113,800

stored at 20° or 30°C, the nucleation rates of both ice water and dry ice CO_2 clusters must be examined. According to the classical nucleation theory, the nucleation energy barrier ΔG^* to overcome the corresponding critical radius r^* needed for a cluster to spontaneously grow through condensation of water vapor or gas-phase CO_2 and the nucleation rate for homogeneous nucleation J_{hom} (defined as the number of clusters that grow past the critical radius r^* per unit volume and per unit time) express as follows (*13*, *14*)

$$\begin{cases} \Delta G^* = \dfrac{16\pi\sigma^3 v_S^2}{3(k_B T \ln S)^2} \\ r^* = \dfrac{2\sigma v_S}{k_B T \ln S} \\ J_{hom} = N_G \dfrac{\rho_V}{\rho_S} \left(\dfrac{2\sigma}{\pi m} \right)^{1/2} \exp\left(-\dfrac{\Delta G^*}{k_B T} \right) \end{cases} \quad (3)$$

with σ being the corresponding surface energy of ice water or dry ice CO_2, v_S being the corresponding volume of a single molecule in the solid phase, k_B being the Boltzmann constant, S being the saturation ratio of the corresponding species in the gas mixture (water vapor or gas-phase CO_2), m being the mass of a single molecule, ρ_V being the density of the corresponding specie in the gas mixture (water vapor or gas-phase CO_2), ρ_S being the density of the solid phase (ice water or dry

ice CO_2) in the clusters, and N_G being the molecular concentration of the corresponding specie in the gas mixture (i.e., $P_{vap}^{H_2O/CO_2}/k_BT$, in m^{-3}).

All the strongly bottle temperature–dependent parameters of the CO_2/H_2O gas mixture (immediately after adiabatic expansion) are presented in table S1, as a function of the bottle's temperature. With nucleation rates of $\approx 6 \times 10^{19}$ cm^{-3} s^{-1} (for bottles stored at 20°C) and $\approx 5 \times 10^{20}$ cm^{-3} s^{-1} (for bottles stored at 30°C), the homogeneous nucleation of ice water clusters is very likely to occur whatever the bottle's temperature. Nevertheless, with homogeneous nucleation rates close to zero for dry ice CO_2 clusters, the freezing of gas-phase CO_2 through homogeneous nucleation remains thermodynamically impossible for the bottles stored at 20° and 30°C (despite saturation ratios substantially higher than 1 for gas-phase CO_2 after adiabatic expansion). In a previous article, the following scenario was proposed to account for the formation of a blue haze as observed above the bottlenecks of a 20°C cork popping bottle (*11*). After adiabatic expansion of the CO_2/H_2O gas mixture, clusters of ice water appear in the bottlenecks through homogeneous nucleation (given their very high rate of homogeneous nucleation). The saturation ratio of gas-phase CO_2 being significantly higher than 1, the freezing of gas-phase CO_2 through heterogeneous nucleation on ice water clusters nuclei becomes therefore thermodynamically possible. Blue haze is nevertheless evidence that dry ice CO_2 clusters remain much smaller in size than the wavelengths of ambient light (centered on 0.6 μm) to allow the Rayleigh scattering of light.

After adiabatic expansion of the CO_2/H_2O gas mixture, the homogeneous nucleation rate of ice water clusters is about eight times higher for the bottles stored at 30°C than that determined for the bottles stored at 20°C. Thus, after an identical period of time following cork popping, ice water nuclei available to allow the freezing of gas-phase CO_2 through heterogeneous nucleation are about eight times more likely above the bottlenecks of bottles stored at 30°C than above those stored at 20°C. Therefore, with a number of dry ice CO_2 clusters per unit volume much higher in the CO_2 freezing plume expelled from the bottle stored at 30°C, the plume appears earlier and is optically more opaque, as shown in the time sequences displayed in Fig. 1. Moreover, unlike the deep blue haze observed for the cork popping bottles stored at 20°C and, presumably, because of dry ice CO_2 nuclei smaller in size than the wavelengths of light, the gray-white freezing plume observed for the bottles stored at 30°C is certainly evidence that the dry ice CO_2 clusters that scatter ambient light reach a much bigger size allowing Mie scattering (as clusters become comparable in size than the wavelength of ambient light, i.e., ≈0.6 μm). Supersaturation is classically the driving force for the growth of dry ice CO_2 clusters in the heterogeneous freezing plumes (*15*). Therefore, with a saturation ratio for gas-phase CO_2 about twice higher for the bottles stored at 30°C (see Table 1), dry ice CO_2 clusters logically grow bigger in size in the plume freely expanding from the bottle stored at 30°C, thus probably reaching the critical size needed to achieve the Mie scattering of light regime, as betrayed by the gray-white plume color.

To properly verify the scenario described above and therefore better interpret the color variation between the freezing plumes expanding from the bottlenecks of bottles stored at 20° and 30°C, a "light scattering ratio", noted as S_{sca} and defined hereafter, was introduced

$$S_{sca} = \frac{\Phi_{blue}}{\Phi_{red}} \quad (4)$$

with Φ_{blue} and Φ_{red} being the fluxes of scattered photons corresponding to wavelengths λ = 0.4 μm and λ = 0.8 μm, respectively.

Accordingly, a bluish light is observed if $S_{sca} > 1$, while a scattering ratio $S_{sca} \approx 1$ results in an achromatic scattering of light. We have estimated the fluxes of scattered light by using the Mie scattering theory valid for spherical clusters (*16*). According to our scenario, ice clusters embedded within the CO_2/H_2O freezing plume are represented as tiny spheres with a water ice core coated by a more or less thick layer of dry ice CO_2. Numerical simulations based on a simplified two-stream radiative transfer model were conducted, where the adopted medium thickness is the throat diameter of the bottleneck (≈1.8 cm, corresponding also to the diameter of the CO_2/H_2O freezing plumes gushing from the champagne bottlenecks). The complex refractive indices corresponding to ice water and dry ice CO_2 were found in the literature (*17*, *18*), whereas the volume number density of ice clusters found in the freezing plumes gushing from bottlenecks (for the bottles stored at 20° and 30°C) was estimated by multiplying the homogenous nucleation rate of ice water $J_{hom}^{H_2O}$, for each bottle temperature, by the time elapsed after cork popping (typically 750 μs, for example, corresponding to the tenth frames of the time sequences displayed in Fig. 1). The computation of the light scattering ratio $S_{sca} = \Phi_{blue}/\Phi_{red}$ is initiated by using the critical radius for ice water clusters in the freezing plumes after adiabatic expansion, as given in table S1 (namely, 0.23 and 0.21 nm for the bottles stored at 20° and 30°C, respectively). In the frame of our scenario, the growth of dry ice CO_2 microcrystals begins through heterogeneous nucleation on ice water nuclei previously formed through homogeneous nucleation (given the huge saturation ratios reached by water vapor after adiabatic expansion of the CO_2/H_2O gas mixture). For the bottles stored at 20° and 30°C, we have considered two cases described hereafter: (i) The initial ice water nucleus has the critical radius of ice water (corresponding to the given temperature) before it is coated by a growing layer of dry ice CO_2 and (ii) the ice water nucleus grows from its critical radius to the critical radius of dry ice CO_2 before starting to coat the ice water core with the growing layer of dry ice CO_2.

Results, corresponding to both cases, are displayed in fig. S1. For both temperatures, the light scattered by the population of ice clusters is achromatic for clusters with radii larger than ≈10 nm. Moreover, below a radius close to 1 nm, because of the enhanced role of absorption and the influence of water ice core, the light scattered by the population of ice clusters appears also achromatic or even slightly reddish (because $S_{sca} < 1$). However, note that in this range of clusters' sizes, the scattered fluxes are so small that the scattered light is practically undetectable. Following fig. S1, a bluish scattered light is strongly produced by clusters showing radii ranging between about 2 and 10 nm. We have also displayed panels with the RGB (Red, Green, and Blue) color encoding corresponding to $S_{sca} = 2$ and to $S_{sca} = 11$ (fig. S1A). As shown from these panels, very large light scattering ratios are not required to obtain a blue tint for the scattered light. In view of these simulations, our observations may be understood as follows. The deep blue haze observed for the bottles stored at 20°C would suggest indirect evidence that the CO_2/H_2O ice clusters grow up to characteristic sizes in the order of several nanometers only (i.e., small enough to promote a bluish scattered light, with $S_{sca} > 1$, as shown in Fig. 1A). Nevertheless, the more marked conditions found in the CO_2/H_2O gas mixture expelled from the bottles stored at 30°C allow an almost instantaneous crossing of the "10-nm threshold" for the population of dry ice CO_2 clusters, beyond which an achromatic scattering is observed (i.e., with $S_{sca} \approx 1$), as shown in Fig. 1B.

The transition between the two scattering regimes from a population of CO_2/H_2O ice clusters with typical radii close to 10 nm, as provided by our numerical simulations, may appear relatively small. However, some particular clouds known as polar mesospheric clouds (PMCs) appear white when hit with sunlight (fig. S2). PMCs are made of ice water crystals with typical sizes about 40 to 50 nm only (*19*). Nevertheless, in the PMCs, the scattering objects significantly differ from the sphere and are made of ice water crystals and not dry ice CO_2 clusters with a core of ice water, as proposed in our numerical simulations aimed at interpreting the plume color observed above champagne bottlenecks.

Heterogeneous condensation caused by the presence of multiple gaseous species was already described in the literature and, particularly, in operational rocket plume exhausts that typically consist in mixtures of simple gaseous species (*20*–*25*). Initial nuclei can be created out of the more easily condensable trace species through homogeneous nucleation, followed by heterogeneous condensation of the less condensable species. At a smaller scale indeed, we believe that champagne bottlenecks could be viewed as small rocket nozzles as the CO_2/H_2O gas mixture, initially under pressure in the sealed bottleneck, freely expands during the cork popping process. In addition, from a phenomenological perspective, the parallel between the CO_2/H_2O gas mixture freely expanding from a champagne bottleneck while cork popping and the phenomena arising in a rocket plume exhaust does not stop here. Closer examination of the freezing plumes freely expelled from the throat of champagne bottlenecks revealed another notable feature well known in aircraft and aerospace engineering, as described in the following paragraph.

Evanescent Mach disks in the under-expanded freezing jets

Gaseous jets may occur whenever a gas phase is exhausted from a reservoir (through a nozzle exit) at a pressure greater than the ambient pressure into which the jet is exhausting (*26*). At the nozzle exit, assuming adiabatic expansion, the Mach number M of the jet (defined as the ratio of the local flow velocity to the local velocity of sound) can be expressed as a function of both the reservoir–to–jet pressure ratio and the ratio of specific heats of the gas mixture experiencing adiabatic expansion according to the following relationship (*27*)

$$M = \left(\frac{2}{\gamma - 1}\right)^{1/2} \left[\left(\frac{P_R}{P_0}\right)^{\frac{\gamma-1}{\gamma}} - 1\right]^{1/2} \quad (5)$$

with P_R being the pressure of gas phase in the reservoir and P_0 being the ambient pressure into which the jet is exhausting.

The Mach number of the flow velocity at the nozzle exit therefore reaches one when the reservoir–to–ambient pressure ratio overcomes the critical ratio defined hereafter

$$\frac{P_R}{P_0} = \left(\frac{\gamma + 1}{2}\right)^{\frac{\gamma}{\gamma-1}} \quad (6)$$

For a reservoir under a pressure of gas-phase CO_2, for example (with $\gamma = 1.3$), this critical pressure ratio is $P_R/P_0 \approx 1.83$. When this situation arises, the jet is said to be under-expanded and the flow exiting the nozzle will tend to expand supersonically, adjusting to the ambient pressure through a system of expansions and shock cells within the jet. The flow geometry associated with under-expanded jets has been investigated for several decades, and their steady-state structure is now well understood (*28*–*32*). Moreover, for highly under-expanded jets exhausting from nozzles with a reservoir–to–ambient pressure ratio greater than about 5, visually appealing series of normal shockwaves (called Mach disks) will also be present along the jet (*29*, *31*). Mach disks are named after Ernst Mach, the Austrian physicist and philosopher who first described them (*33*). Highly under-expanded jets are indeed involved in practical engineering situations, such as exhausts and plumes of aircrafts and aerospace rockets, where the thermal signature, jet noise, and flow behavior were carefully studied in the past decades (*34*–*36*). The gaseous exhaust is expelled from the engine supersonically, where it is under-expanded adiabatically to form a well-collimated jet that remains stable over a distance many times as long as its diameter (*26*). A wonderful illustration of the occurrence of Mach disks in the supersonic exhausts of a fighter aircraft can be seen in Fig. 3. More information about the overall structure of under-expanded jets in a quiescent medium, including the main features of Mach disks (apparition, position, and diameter), can be found in a recent review by Franquet *et al.* (*35*).

From a phenomenological point of view, the CO_2/H_2O gas mixture initially under pressure in the headspace of the champagne corked bottle freely expands through the throat of the bottleneck into ambient air while cork popping. In our cork popping experiments, the initial reservoir–to–ambient pressure ratio much exceeds the critical ratio needed to reach Mach 1 (equal to 1.83 for gas-phase CO_2), resulting in the formation of under-expanded jets. Moreover, in our experiments, the cork popping situation initially shows a reservoir–to–ambient pressure ratio greater than 5 (7.5 for the bottles stored at 20°C against 10.2 for those stored at 30°C), which seems to be the order of magnitude of the critical pressure ratio needed for the formation of Mach disks (*29*, *31*). A close-up time sequence showing details of the freezing plume accompanying the cork popping process of a bottle stored at 20°C is displayed in Fig. 4 (and in movie S1). A Mach disk shock normal to the flow appears on Fig. 4A about 580 μs after cork popping. The Mach disk then progressively moves away from the bottleneck, as seen from Fig. 4 (A to D). It seems to get back toward the bottleneck in Fig. 4E, and it finally vanishes in Fig. 4F about 1 ms after cork popping.

Mach disks and their characteristics are certainly the most studied features in the literature devoted to under-expanded jets, be it experimentally, theoretically, or numerically, as presented in the exhaustive and recent overview by Franquet *et al.* (*35*). Among the huge amount of studies devoted to this feature, the location of the Mach disk with regard to the nozzle exit or vent was particularly investigated. On the largest range of reservoir–to–ambient pressure ratio, the location of the

Fig. 3. Evidence for evenly spaced Mach disks in the supersonic exhausts of a pair of U.S. Air Force F-15E Strike Eagles flying over northern Iraq (credit: U.S. Air Force/Senior Airman Matthew Bruch).

Mach disk shock was first predicted by Crist *et al.* (*37*), according to the following relationship

$$\frac{L}{D} = 0.65 \left(\frac{P_R}{P_0}\right)^{1/2} \quad (7)$$

with L being the standoff distance of the Mach disk shock from the nozzle exit, D being the throat diameter of the nozzle, and P_R/P_0 being the reservoir–to–ambient pressure ratio.

In Fig. 5, the standoff distance of the Mach disk shocks from the bottleneck's throat is plotted as a function of time for the bottles stored at 20° and 30°C, respectively. Applying the latter equation to the case of our cork popping experiments, with a bottleneck throat diameter of $D \approx$ 1.8 cm and with reservoir–to–ambient pressure ratios close to 7.5 and 10.2 (whether the bottles were stored at 20° or 30°C), leads to standoff distances of the Mach disk shocks lying approximately 3.2 and 3.7 cm, respectively, from the bottleneck's throat. These distances are indeed much higher than those experimentally observed (Fig. 5). But actually, Eq. 7 was determined for unconfined under-expanded supersonic jets freely exhausting in an unbounded infinite atmosphere. In our cork popping experiments, the CO_2/H_2O gas mixture is underexpanding in ambient air but in the presence of the cork, which is flying with a velocity (≈15 m s^{-1}) much less than that of the jet (*9*). The gaseous jet following cork popping finally differs from an unconfined under-expanded supersonic jet and rather corresponds to a supersonic jet impinging on a flat obstacle normal to the flow. It was indeed already reported that a supersonic jet impinging on a plate normal to the flow increases the static pressure downstream of the Mach disk shock (*28*, *38*–*40*). In normal impingement, an outflow parallel to the plate therefore develops the so-called wall jet (*39*), which is visible on both sides of the flying cork base in Fig. 4. Because of this effect, the Mach disk shock standoff distance was found to decrease with decreasing separation distance between the plate and the nozzle from which the gaseous jet is exhausting (*41*). It seems self-consistent with our observations indicating that the standoff distance of the Mach disk shock from the throat of the bottleneck is indeed much less than predicted from Eq. 7 and that it progressively increases as a function of time (Fig. 5). The Mach disk shock standoff distance progressively increasing from the throat of the bottleneck should be a consequence of the increasing separation distance between the flying cork base and the throat of the bottleneck from which the CO_2/H_2O gas mixture is exhausting.

Otherwise, because the champagne bottleneck has a very small finite volume close to 25 ml, the reservoir–to–ambient pressure ratio quickly decreases as a function of time and should inevitably go below the critical pressure ratio needed for the formation of Mach disks (which were de facto seen vanishing approximately in the very first millisecond after cork popping for the bottles stored at 20° and 30°C, as shown in Figs. 1 and 4). In case of finite overpressurized reservoirs expelling a jet of gas through a nozzle, and assuming an isentropic process, the decreasing with time t of the reservoir–to–ambient pressure ratio was determined according to the following relationship (*42*)

$$\frac{P_R(t)}{P_0} = \frac{P_R^0}{P_0}\left(\frac{tc_R S_B}{V_R}\left[\left(\frac{\gamma-1}{2}\right)\left(\frac{2}{\gamma+1}\right)^{\frac{\gamma+1}{2(\gamma-1)}}\right]+1\right)^{\frac{2\gamma}{1-\gamma}} \quad (8)$$

with P_R^0 being the initial pressure of gas phase in the reservoir (namely, 7.5 and 10.2 bar in the present case for the bottles stored at 20° and 30°C, respectively), V_R being the reservoir volume (≈25 ml in the present case), S_B being the nozzle area (≈2.5 cm^2 in the present case), and c_R being the sound speed in the reservoir (i.e., $c_R = \sqrt{\gamma RT/M}$, with M = 44 g mol^{-1} being the molar mass of gas phase in the reservoir, indeed mainly composed of gas-phase CO_2).

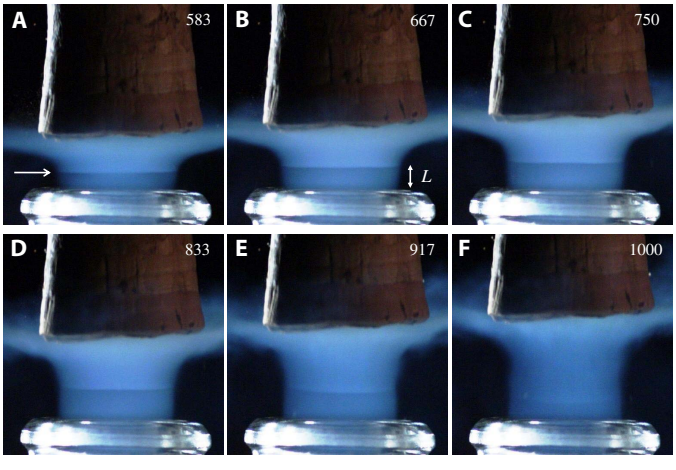

Fig. 4. Details of the freezing jet expelled from the bottleneck of a bottle stored at 20°C. A Mach disk shock normal to the flow appears in (**A**), about 580 μs after cork popping (white arrow). The standoff distance L of the Mach disk to the throat of the bottleneck then progressively increases from (A) to (**D**). It seems to slightly decrease in (**E**) before the Mach disk finally vanishes in (**F**) about 1 ms after cork popping. The time elapsed after cork popping appears in each panel (in microseconds).

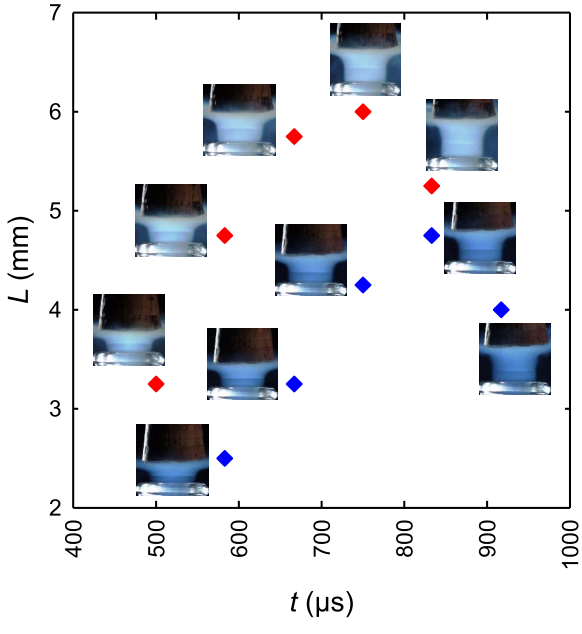

Fig. 5. Standoff distances of the Mach disk to the throat of the bottleneck as a function of the time elapsed since cork popping for the bottles stored at 20° (blue diamond) and 30°C (red diamond). The panel close to each experimental dot refers to the corresponding panel in Fig. 1.

By application of the latter equation, the characteristic time needed to decrease the reservoir–to–ambient pressure ratio below the critical ratio needed to reach Mach 1 (equal to 1.83 for gas-phase CO_2) is equal to 750 μs for the bottle stored at 20°C and to 920 μs for the bottle stored at 30°C. Therefore, the characteristic times needed for the freezing jet expelled from the throat of the bottlenecks to become subsonic (thus precluding the formation of expansions and compression waves within the jet) are in quite good accordance with our experimental observations showing the vanishing of the Mach disks in the very first millisecond following cork popping. It becomes also possible to compare the standoff distance of the Mach disk shocks from the bottleneck's throat, with the scaling law predicted by Crist *et al.* (*37*), by including in Eq. 7 the dependence with time of the reservoir–to–ambient pressure ratio given by Eq. 8. The location of the Mach disk shock normalized by the diameter of the bottleneck (for the bottles stored at 20° and 30°C) is compared with the scaling law predicted from Eq. 7 (fig. S3). As time proceeds, the flying cork moves away from the throat of the bottlenecks, and our experimental data progressively tend toward the scaling law predicted in (*37*) (determined for unconfined under-expanded supersonic jets). The decreasing influence of the cork is thus evidenced as it moves away from the throat of the bottleneck.

Mach disks were already observed within a jet exhausting from the bottleneck of a plastic soft drink bottle that was pressurized with air on a toy pneumatic rocket launcher (*43*). A high-speed schlieren video device was used to visualize refractive index gradients within the under-expanded jet, as captured by P. Petersen in fig. S4. After launch, the air jet exhausting the throat of the bottleneck is underexpanding into ambient air at a speed near Mach 1. Far from the launcher, and therefore under unconfined conditions, a series of evenly spaced Mach disks can be observed. Under these unconfined conditions, the distance from the throat of the bottleneck to the first Mach disk is in the order of 2.5 cm, as predicted by Eq. 7. Nevertheless and contrary to most of the better controlled steady flow experiments reported in the literature, the champagne cork popping process is a highly unsteady flow process, with a very quickly time decreasing reservoir–to–ambient pressure ratio and with the base of the flying cork acting as a small plate moving away from the throat of the bottlenecks from which the under-expanded freezing jet is expelled. Two-dimensional computational fluid dynamics simulations based on the resolution of the Navier-Stokes equations would certainly help to a better understanding of the structure of the flow field in the presence of the cork.

CONCLUSION

During champagne cork popping, the CO_2/H_2O gas mixture initially under pressure in the headspace of the bottle freely expands into ambient air and experiences adiabatic cooling. A comparison between the condensation phenomena accompanying cork popping from bottles stored at 20° and 30°C was made. The initial headspace–to–ambient-pressure ratio (7.5 for the bottles stored at 20°C against 10.2 for those stored at 30°C) much exceeded the critical ratio needed for the CO_2/H_2O gas mixture to reach Mach 1, thus forming under-expanded supersonic jets expelled from the throat of the bottlenecks. Unlike the deep blue haze observed for the bottles stored at 20°C and, presumably, because of CO_2 heterogeneous freezing with dry ice CO_2 nuclei smaller in size than the wavelengths of light, the plume freely expanding from the bottles stored at 30°C turned gray-white. After adiabatic expansion, with a saturation ratio for gas-phase CO_2 about twice higher for the bottles stored at 30°C, dry ice CO_2 clusters logically grow bigger in size, thus probably reaching the critical size needed to achieve the Mie scattering of light and turn gray-white. Moreover, during the first millisecond following the cork popping process, normal shock waves (or Mach disks) were unveiled in the under-expanded CO_2 freezing plumes exhausted from the throat of champagne bottlenecks until the reservoir–to–ambient pressure ratio goes below a critical ratio needed for the formation of Mach disks, which were de facto seen vanishing about 1 ms after cork popping. The application of high-speed schlieren technology, which relies on the refractive index of a transparent medium changing with density to produce an image, could be used in a near future to better understand the cork popping process of champagne and sparkling wines. Visualizing the under-expanded jets expelled from the throat of bottlenecks with such a technology could help us achieve a clearer picture of the subsequent formation and dynamics of shock waves accompanying the cork popping process.

MATERIALS AND METHODS

Thermodynamic equilibrium of gas-phase CO_2 and water vapor in the sealed bottles

A single batch of six champagne rosé bottles (Vranken Pommery, Marne, France) with 12.5% (v/v) ethanol, elaborated with a blend of chardonnay and pinot noir base wines in standard 75-cl clear transparent bottles, was used for this set of experiments. It is noteworthy to mention that 72 hours before each set of experiments, bottles were stored at the desired temperature (four bottles at 20°C and the two others at 30°C). To promote the in-bottle second alcoholic fermentation (or prise de mousse), yeasts along with sugar (24 g $liter^{-1}$) were classically added in the bottles hermetically sealed with a crown cap. The key metabolic process behind the production of gas-phase CO_2 in the sealed bottles is alcoholic fermentation (i.e., the conversion of sugars into ethanol and CO_2 by yeast). Sugar (24 g $liter^{-1}$) added in the blend leads to the production of 8.8 g of CO_2 (or 0.2 mol) in every bottle of champagne (*6*). Moreover, because the capacity of CO_2 to dissolve in champagne is ruled by the so-called Henry's law equilibrium, the concentration of dissolved CO_2 in the liquid phase is proportional to the partial pressure of gas-phase CO_2 in the headspace of the sealed bottle. Therefore, the following relationship applies

$$C_L = \frac{n_L}{V_L} = k_H P \tag{9}$$

with n_L being the mole number of dissolved CO_2 in the liquid phase, V_L being the volume of the liquid phase in the sealed bottle, P being the partial pressure of gas-phase CO_2 in the sealed bottle, and k_H being the strongly temperature-dependent Henry's law constant of gas-phase CO_2 in the liquid phase, conveniently expressed with the van't Hoff–like equation as follows (*44*)

$$k_H(T) = k_{298K} \exp\left[-\frac{\Delta H_{diss}}{R}\left(\frac{1}{T} - \frac{1}{298}\right)\right] \tag{10}$$

with $k_{298K} \approx 1.21$ g $liter^{-1}$ bar^{-1}, $\Delta H_{diss} \approx 24.8$ kJ mol^{-1} being the dissolution enthalpy of CO_2 molecules in the liquid phase (*44*), R being the ideal gas constant (8.31 J K^{-1} mol^{-1}), and T being the absolute temperature (in K).

After the prise de mousse, bottles aged in a cool cellar for 42 months. Bottles were then disgorged, which consists in opening the bottles to remove the dead yeast cells and recorking them with traditional natural cork stopper (provided by Amorim & Irmãos, Portugal). During the disgorging process, a bit of CO_2 is inevitably lost at this step as gas-phase CO_2 escapes from the bottleneck under the action of pressure when opening the bottle. The thermodynamic equilibrium of CO_2 is broken, but dissolved and gas-phase CO_2 quickly recover Henry's equilibrium in the recorked bottle where a volume V_G of gas phase (the headspace) still cohabits with the volume V_L of champagne (i.e., the liquid phase). Note that into every bottle of this batch, the volume V_G of gas phase in the headspace under the cork is close to 25 ml, whereas the volume V_L of champagne (i.e., the liquid phase) is 75 cl. Recently, the following relationship was theoretically determined for the newly recovered equilibrium pressure of gas-phase CO_2 in the corked bottles after the disgorging step was achieved (denoted as $P_{CB}^{CO_2}$ and expressed in Pa) (*11*)

$$P_{CB}^{CO_2} \approx \frac{n_T k_H (RT)^2 V_L}{(V_G + k_H RT V_L)^2} \quad (11)$$

with n_T being the total number of CO_2 moles produced in a sealed bottle after the prise de mousse (i.e., 0.2 mol in the present case).

Otherwise, in the sealed medium of a corked champagne bottle, the water vapor in the headspace under the cork is indeed under equilibrium with the liquid-phase water found in champagne. Above the melting point of water, the strongly temperature-dependent saturated water vapor pressure $P_{sat}^{H_2O}$ is accurately determined according to the following Antoine equation

$$\mathrm{Log}_{10}(P_{sat}^{H_2O}) = A - \frac{B}{T + C} \quad (12)$$

with $P_{sat}^{H_2O}$ being expressed in mmHg, T being expressed in °C, and the coefficients A, B, and C being provided by the National Institute of Standards and Technology database. In the range of temperatures comprised between 1° and 99°C, Antoine coefficients A, B, and C are 8.07131, 1730.63, and 233.426, respectively (*45*).

The volume fraction of liquid-phase water, denoted as $x_L^{H_2O}$, is close to 0.87 for our champagne samples at 12% (v/v) ethanol. The pressure of water vapor in the sealed bottle is therefore expressed as $P_{CB}^{H_2O} \approx x_L^{H_2O} P_{sat}^{H_2O}$. In Fig. 2, the respective partial pressures of gas-phase CO_2 and water vapor found in a champagne corked bottle, as determined in accordance with the thermodynamic equilibrium described above, are plotted as a function of the bottle's temperature T. As shown in Fig. 2, the temperature-dependent partial pressure of gas-phase CO_2 is more than two orders of magnitude higher than that of water vapor pressure, and the total pressure of the CO_2/H_2O gas mixture found in the sealed champagne bottles is therefore considered as being equivalent to the partial pressure of gas-phase CO_2. For the sake of simplicity, it will be denoted as P_{CB} in the article.

Temperature dependences of ice water and dry ice CO_2–saturated vapor pressures

Below the melting point of water, at temperatures between 170 and 250 K (i.e., between −103° and −23°C), which perfectly covers the range of temperatures reached by the gas mixture freely expanding above the bottleneck during the cork popping process, the vapor pressure of ice water $P_{sat}^{H_2O}$ was found to obey the following relationship (*46*)

$$P_{sat}^{H_2O} = \exp\left(28.868 - \frac{6132.9}{T}\right) \quad (13)$$

with $P_{sat}^{H_2O}$ being expressed in Pa and T being expressed in K.

Similarly, the relationship between the saturated vapor pressure of gas-phase CO_2 $P_{sat}^{CO_2}$ and temperature T is provided by Antoine equation as follows (*47*)

$$\mathrm{Log}_{10}(P_{sat}^{CO_2}) = A - \frac{B}{T + C} \quad (14)$$

with $P_{sat}^{CO_2}$ being expressed in bar, T being expressed in K, and the coefficients A, B, and C being provided by the NIST database. In the range of temperatures between 154 and 196 K (i.e., between −119° and −77°C), Antoine coefficients A, B, and C are 6.81228, 1301.679, and −3.494, respectively (*45*).

High-speed video device

A digital high-speed cinema camera (Phantom Flex Vision Research, USA) was used for this set of experiments. To get synchronized with the split-second timing of cork popping, the shooting of the camera was posttriggered by using a simple microphone recording the "bang" done by the cork popping from the bottleneck. A 5000-W lamp powered by dc, needed to eliminate the so-called flicker phenomenon, was placed behind the corked bottleneck. A filming rate of 12,000 frames/s at a resolution of 512 × 512 pixels was chosen to examine details of the under-expanded CO_2 freezing jet formed, as the CO_2/H_2O gas mixture (initially under pressure in the sealed champagne bottles) freely expands during the cork popping process.

SUPPLEMENTARY MATERIALS

Supplementary material for this article is available at http://advances.sciencemag.org/cgi/content/full/5/9/eaav5528/DC1

Table S1. Parameters of the CO_2/H_2O gas mixture after adiabatic expansion.
Fig. S1. Numerical simulations of the light scattering ratio.
Fig. S2. Picture of PMCs.
Fig. S3. Location of the Mach disk shock normalized by the diameter of the bottleneck.
Fig. S4. Mach disks formed in the jet exhausting from the bottleneck of a plastic bottle.
Movie S1. High-speed video showing the cork popping process from a bottle stored at 20°C.
Reference (*48*)

REFERENCES AND NOTES

1. D. Archer, N. Galloway, Champagne-cork injury to the eye. *Lancet* **290**, 487–489 (1967).
2. G. M. Cavallini, N. Lugli, L. Campi, L. Pagliani, P. Saccarola, Bottle-cork injury to the eye: A review of 13 cases. *Eur. J. Ophtalmol.* **13**, 287–291 (2003).
3. F. Kuhn, V. Mester, R. Morris, J. Dalma, Serious eye injuries caused by bottles containing carbonated drinks. *Br. J. Ophtalmol.* **88**, 69–71 (2004).
4. D. Sharp, Safe bubbly. *Lancet* **364**, 2165 (2004).
5. G. Liger-Belair, *Uncorked: The Science Of Champagne* (Princeton Univ. Press, Princeton, 2013).
6. G. Liger-Belair, Effervescence in champagne and sparkling wines: From grape harvest to bubble rise. *Eur. Phys. J. Special Topics* **226**, 3–116 (2017).
7. R. Batt, Pop! goes the champagne bottle cork. *J. Chem. Educ.* **48**, 75 (1971).
8. M. Vollmer, K.-P. Möllmann, Vapour pressure and adiabatic cooling from champagne: Slow-motion visualization of gas thermodynamics. *Phys. Educ.* **47**, 608–615 (2012).

9. G. Liger-Belair, M. Bourget, C. Cilindre, H. Pron, G. Polidori, Champagne cork popping revisited through high-speed infrared imaging: The role of temperature. *J. Food Eng.* **116**, 78–85 (2013).
10. A. Sanchez-Lavega, *An Introduction to Planetary Atmospheres* (CRC Press, 2011).
11. G. Liger-Belair, D. Cordier, J. Honvault, C. Cilindre, Unveiling CO_2 heterogeneous freezing plumes during champagne cork popping. *Sci. Rep.* **7**, 10938 (2017).
12. J. G. Speight, *Lange's Handbook of Chemistry* (McGraw-Hill, ed. 17, 2017).
13. F. F. Abraham, *Homogeneous Nucleation Theory* (Academic Press, 1974).
14. R. Zhang, A. Khalizov, L. Wang, M. Hu, W. Xu, Nucleation and growth of nanoparticles in the atmosphere. *Chem. Rev.* **112**, 1957–2011 (2012).
15. S. Yuko, *Statistical Physics of Crystal Growth* (World Scientific, 1996).
16. C. F. Bohren, D. R. Huffman, *Absorption and Scattering of Light by Small Particles* (Wiley-VCH, ed. 2, 2014).
17. S. G. Warren, Optical constants of carbon dioxide ice. *Appl. Opt.* **25**, 2650–2674 (1986).
18. S. G. Warren, R. E. Brandt, Optical constants of ice from the ultraviolet to the microwave: A revised compilation. *J. Geophys. Res.* **113**, D144220 (2008).
19. D. Rusch, G. Thomas, A. Merkel, J. Olivero, A. Chandran, J. Lumpe, J. Carstans, C. Randall, S. Bailey, J. Russell III, Large ice particles associated with small ice water content observed by AIM CIPS imagery of polar mesospheric clouds: Evidence for microphysical coupling with small-scale dynamics. *J. Atmos. Sol. Terr. Phys.* **162**, 97–105 (2017).
20. B. E. Wyslouzil, C. H. Heath, J. L. Cheung, G. Wilemski, Binary condensation in a supersonic nozzle. *J. Chem. Phys.* **113**, 7317–7329 (2000).
21. A. Moudens, R. Georges, M. Goubet, M. J. Makarewicz, S. E. Lokshtanov, A. A. Vigasin, Direct absorption spectroscopy of water clusters formed in a continuous slit nozzle expansion. *J. Chem. Phys.* **131**, 204312 (2009).
22. Z. Li, J. Zhong, D. A. Levin, Modeling of CO_2 homogeneous and heterogeneous condensation plumes. *J. Phys. Chem. C* **114**, 5276–5286 (2010).
23. O. F. Hagena, W. Obert, Cluster formation in expanding supersonic jets: Effect of pressure, temperature, nozzle size, and test gas. *J. Chem. Phys.* **56**, 1793–1802 (1972).
24. A. Ramos, J. M. Fernández, G. Tejeda, S. Montero, Quantitative study of cluster growth in free-jet expansions of CO_2 by Rayleigh and Raman scattering. *Phys. Rev. A* **72**, 053204 (2005).
25. J. Zhong, M. I. Zeifman, D. A. Levin, Kinetic model of condensation in a free argon expanding jet. *J. Thermophys. Heat Transfer* **20**, 41–51 (2006).
26. M. Norman, K.-H. Winkler, Supersonic jets. *Los Alamos Sci.* **12**, 38–71 (1985).
27. M. A. Saad, *Compressible Fluid Flow* (Prentice Hall, 1993).
28. C. d. Donaldson, R. S. Snedeker, A Study of free jet impingement. Part 1. Mean properties of free and impinging jets. *J. Fluid Mech.* **45**, 281–319 (1971).
29. T. Irie, T. Yasunobu, H. Kashimura, T. Setoguchi, Characteristics of the mach disk in the underexpanded jet in which the back pressure continuously changes with time. *J. Therm. Sci.* **12**, 132–137 (2003).
30. A. Risborg, J. Soria, High-speed optical measurements of an underexpanded supersonic jet impinging on an inclined plate, in *28th International Congress on High-Speed Imaging and Photonics* (SPIE, 2009), vol. 7126, p. 71261F.
31. M. M. Orescanin, J. M. Austin, Exhaust of underexpanded jets from finite reservoirs. *J. Propul. Power* **26**, 744–753 (2010).
32. M. M. Orescanin, D. Prisco, J. M. Austin, S. W. Kieffer, Flow of supersonic jets across flat plates: Implications for ground-level flow from volcanic blasts. *J. Geophys. Res. Sol. Earth* **119**, 2976–2987 (2014).
33. E. Mach, Uber den Verlauf von Funkenwellen in der Ebene und im Raume. *Sitzungsbr. Akad. Wien* **78**, 819–838 (1878).
34. B. André, T. Castelain, C. Bailly, Experimental exploration of underexpanded supersonic jets. *Schock Waves* **24**, 21–32 (2014).
35. E. Franquet, V. Perrier, S. Gibout, P. Bruel, Free underexpanded jets in a quiescent medium: A review. *Prog. Aerosp. Sci.* **77**, 25–53 (2015).
36. V. Zapryagaev, N. Kiselev, D. Gubanov, Shock-wave structure of supersonic jet flows. *Aerospace* **5**, 60 (2018).
37. S. Crist, P. M. Sherman, D. R. Glass, Study of the highly underexpanded sonic jet. *AIAA J.* **4**, 68–71 (1966).
38. J. C. Carling, B. L. Hunt, The Near wall jet of a normally impinging, uniform, axisymmetric, supersonic jet. *J. Fluid Mech.* **66**, 159–176 (1974).
39. P. J. Lamont, B. L. Hunt, The impingement of underexpanded, axisymmetric jets on perpendicular and inclined flat plates. *J. Fluid Mech.* **100**, 471–511 (1980).
40. J.-C. Lengrand, J. Allègre, M. Raffin, Underexpanded free jets and their interaction with adjacent surfaces. *AIAA J.* **20**, 27–28 (1982).
41. I. Khalil, D. R. Miller, The structure of supercritical fluid free-jet expansions. *AIChE J.* **50**, 2697–2704 (2004).
42. S. W. Kieffer, B. Sturtevant, Laboratory studies of volcanic jets. *J. Geophys. Res.* **89**, 8253–8268 (1984).
43. "Even a soda bottle rocket can do one of a fighter jet's coolest tricks," *Popular Mechanics*, 22 March 2017; www.popularmechanics.com/science/a25777/soda-bottle-rocket-shock-diamonds/.
44. G. Liger-Belair, The physics and chemistry behind the bubbling properties of champagne and sparkling wines: A state-of-the-art review. *J. Agric. Food Chem.* **53**, 2788–2802 (2005).
45. O. C. Bridgeman, E. W. Aldrich, Vapor pressure tables for water. *J. Heat Transfer* **86**, 279–286 (1964).
46. J. Marti, K. A. Mauersberger, A survey and new measurements of ice vapor pressure at temperatures between 170 and 250K. *Geophys. Res. Lett.* **20**, 363–366 (1993).
47. W. F. Giauque, C. J. Egan, Carbon dioxide. The heat capacity and vapor pressure of the solid. The heat of sublimation. Thermodynamic and spectroscopic values of the entropy. *J. Chem. Phys.* **5**, 45–54 (1937).
48. A. Määttänen, H. Vehkamäki, A. Lauri, S. Merikallio, J. Kauhanen, H. Savijärvi, M. Kulmala, Nucleation studies in the Martian atmosphere. *J. Geophys. Res.* **110**, E02002 (2005).

Acknowledgments: We acknowledge T. Gasco, chef de cave from Champagne Pommery, for providing us with the batch of champagne rosé used in this set of experiments. We are also indebted to the Association Recherche Œnologique Champagne et Université (AROCU) for moral support. **Funding:** There are no funding sources for this research. **Author contributions:** G.L.-B. designed and performed research. G.L.-B., D.C., and R.G. analyzed data. G.L.-B. wrote the paper with inputs from all co-authors. All authors discussed the results and commented on the manuscript. **Competing interests:** The authors declare that they have no competing interests. **Data and materials availability:** All data needed to evaluate the conclusions in the paper are present in the paper and/or the Supplementary Materials. Additional data related to this paper may be requested from the authors.

Submitted 27 September 2018
Accepted 19 August 2019
Published 20 September 2019
10.1126/sciadv.aav5528

Citation: G. Liger-Belair, D. Cordier, R. Georges, Under-expanded supersonic CO_2 freezing jets during champagne cork popping. *Sci. Adv.* **5**, eaav5528 (2019).

Science Advances

Under-expanded supersonic CO_2 freezing jets during champagne cork popping

Gérard Liger-Belair, Daniel Cordier and Robert Georges

Sci Adv **5** (9), eaav5528.
DOI: 10.1126/sciadv.aav5528

Science Advances (ISSN 2375-2548) is published by the American Association for the Advancement of Science, 1200 New York Avenue NW, Washington, DC 20005. The title *Science Advances* is a registered trademark of AAAS.